

## Electronic Supplementary Information

---

### Experimental

*Synthesis of Co-Co PBA microcubes.* The uniform Co-Co PBA microcubes with size of 900 nm were synthesized by a simple precipitation method. In a typical procedure, 0.6 mmol of cobalt acetate and 0.9 mmol of sodium citrate were dissolved in 20 mL of deionized (DI) water to form solution A. At the same time, 0.4 mmol of potassium hexacyanocobaltate(III) was dissolved in 20 mL of DI water to form solution B. Then, solutions A and B were mixed together under magnetic stirring for 1 min. The obtained mixed solution was aged for 12 h at room temperature. After collected by centrifugation and washed with water and ethanol, the precipitates were dried at 70 °C overnight.

*Synthesis of Co-Co PBA microframes.* In a typical synthesis, 10 mg of the above as-prepared Co-Co PBA microcubes were dissolved in 10 mL of ethanol with the assistance of ultrasonication for 15 min to form solution C. 5 mL of ammonia solution were dissolved in 15 mL of water to form solution D. Then, solutions C and D were mixed together and the mixture was stirring at room temperature for 10 min. The final products were collected by centrifugation, and washed with DI water and ethanol for three times, before drying at 70 °C overnight. Preliminary experimental results showed that it is hard to control the etching rate with more higher concentration of ammonia solution, while lower concentration of ammonia solution will lead to much longer etching time. Therefore, 5 mL of ammonia solution were chosen as the etchant.

*Synthesis of Co<sub>3</sub>O<sub>4</sub> microframes.* In a typical synthesis, the as-prepared Co-Co PBA microframes were annealed at 600 °C for 2 h with a heating temperature rate of 2 °C min<sup>-1</sup> in air. For comparison, the as-prepared Co-Co PBA microcubes were also annealed to prepare Co<sub>3</sub>O<sub>4</sub>

microcubes under the same experimental conditions. Preliminary experimental results showed that when the calcination temperature is lower than 600 °C,  $\text{Co}_3\text{O}_4$  with poor crystallinity will be obtained, while higher calcination temperature than 600 °C will lead to the collapse of  $\text{Co}_3\text{O}_4$  microframes. Therefore, 600 °C was chosen as the calcination temperature.

*Materials characterization.* The crystal phase of the products was examined by X-ray diffraction (XRD) on a Rigaku D/MAX RINT-2000 X-Ray Diffractometer. Field-emission scanning electron microscope (FESEM; JEOL-7600F) and transmission electron microscope (TEM; JEOL, JEM-2100F) were used to examine the morphology of the samples. Thermogravimetric analysis (TGA) was performed with a temperature ramp of 10 °C  $\text{min}^{-1}$  under air flow. Fourier transform-infrared spectroscopy (FT-IR) was carried out on a Nicolet 5700 FT-IR Spectrometer. The specific surface areas of as-synthesized materials are measured on Autosorb-1 at liquid-nitrogen temperature.

*Electrochemical measurements.* The battery tests were carried out in a half-cell configuration. The working electrode consists of active materials, conductivity agent (Kejten black, KB), and polymer binder (polyvinylidene fluoride, PVDF) with a weight ratio of 70:20:10. The electrolyte is 1 M  $\text{LiPF}_6$  in a mixture of ethylene carbonate and diethyl carbonate (1:1 by weight). The loading mass of active materials is around 1.0  $\text{mg cm}^{-2}$ . Lithium disc was used as both the counter electrode and reference electrode. The coin-type half cells were assembled in argon-filled glove box and then tested in TOSCAT 3000 battery tester (TOSCAT 3000, Toyo Systems, Tokyo, Japan) with a voltage range between 0.01 and 3 V. Cyclic Voltammetry (CV) curves were tested using AUTOLAB potentiostat/galvanostat apparatus (AUT85698). The OER activity was evaluated in a three-electrode configuration using a rotating disk electrode (RDE) (Autolab RDE/2, at a rotation speed of 1700 rpm) with an Autolab potentiostat/galvanostat (Model

PGSTAT-72637) workstation at ambient temperature. A glassy carbon electrode (GCE) with a diameter of 3 mm was used as the support for the working electrode. The catalyst suspension was prepared by dispersing 5 mg of catalyst in 1 mL of solution containing 0.5 mL of DI water, 0.44 mL of ethanol and 60  $\mu\text{L}$  of 0.5 wt.% Nafion solution followed by ultrasonication for 30 min. 4  $\mu\text{L}$  of the catalyst suspension was pipetted onto the GCE surface using a micropipettor and then dried at ambient temperature. The catalyst loading amount is 0.286  $\text{mg cm}^{-2}$  on the GCE. A Ag/AgCl (KCl saturated) electrode was used as the reference electrode and a platinum disc electrode was used as the counter electrode. Potentials were referenced to a reversible hydrogen electrode (RHE):  $E(\text{RHE}) = E(\text{Ag}/\text{AgCl}) + (0.2 + 0.059 \text{ pH})\text{V}$ . Linear sweep voltammetry (LSV) was recorded in 1 M KOH ( $\text{pH} = 13.56$ ) at a scan rate of 5  $\text{mV s}^{-1}$  to obtain the polarization curves. The long-term stability tests were performed by continuous LSV scans with a sweep rate of 50  $\text{mV s}^{-1}$ . All the data presented were corrected for  $iR$  losses and background current. EIS was performed at overpotential of 370 mV with frequency from 0.1 to 100,000 Hz and an amplitude of 5 mV. The electrochemical double-layer capacitance was determined from the CV curves measured in a potential range without redox processes according to the following equation:  $C_{\text{dl}} = I_c/v$ , where  $C_{\text{dl}}$ ,  $I_c$ , and  $v$  are the double-layer capacitance ( $\text{F cm}^{-2}$ ) of the electroactive materials, charging current ( $\text{mA cm}^{-2}$ ), and scan rate ( $\text{mV s}^{-1}$ ), respectively.

**Table S1.** Comparison of LIBs performance of different Co<sub>3</sub>O<sub>4</sub>-based anodes.

Electrode materials	Cycling performance	Rate capability	References
<b>Co<sub>3</sub>O<sub>4</sub> microframes</b>	<b>1296 mAh g<sup>-1</sup> after 200 cycles at 500 mA g<sup>-1</sup></b>	<b>953 mAh g<sup>-1</sup> at 1 A g<sup>-1</sup></b>	<b>This work</b>
	<b>757 mAh g<sup>-1</sup> after 4000 cycles at 5000 mA g<sup>-1</sup></b>	<b>883 mAh g<sup>-1</sup> at 2 A g<sup>-1</sup></b> <b>620 mAh g<sup>-1</sup> at 8 A g<sup>-1</sup></b>	
PBA-derived Co <sub>3</sub> O <sub>4</sub> nanocages	970 mAh g <sup>-1</sup> after 30 cycles at 50 mA g <sup>-1</sup>	252 mAh g <sup>-1</sup> at 2 A g <sup>-1</sup>	1
PBA-derived Fe <sub>2</sub> O <sub>3</sub> /Co <sub>3</sub> O <sub>4</sub> hollow microcubes	500 mAh g <sup>-1</sup> after 50 cycles at 100 mA g <sup>-1</sup>	272 mAh g <sup>-1</sup> at 0.8 A g <sup>-1</sup>	2
MOF-derived agglomerated Co <sub>3</sub> O <sub>4</sub> nanoparticles	965 mAh g <sup>-1</sup> after 50 cycles at 50 mA g <sup>-1</sup>	Unavailable	3
Co <sub>3</sub> O <sub>4</sub> hexagonal nanorings	1370 mAh g <sup>-1</sup> after 30 cycles at 100 mA g <sup>-1</sup>	1335 mAh g <sup>-1</sup> at 1 A g <sup>-1</sup>	4
Nanocage Co <sub>3</sub> O <sub>4</sub>	810 mAh g <sup>-1</sup> after 100 cycles at 500 mA g <sup>-1</sup>	712 mAh g <sup>-1</sup> at 1 A g <sup>-1</sup>	5
Graphene/Co <sub>3</sub> O <sub>4</sub> ultrafine nanocrystallites	714 mAh g <sup>-1</sup> after 200 cycles at 200 mA g <sup>-1</sup>	877 mAh g <sup>-1</sup> at 5 A g <sup>-1</sup>	6
Mesoporous nanostructured Co <sub>3</sub> O <sub>4</sub>	913 mAh g <sup>-1</sup> after 60 cycles at 200 mA g <sup>-1</sup>	442 mAh g <sup>-1</sup> at 1 A g <sup>-1</sup>	7
MWCNTs/Co <sub>3</sub> O <sub>4</sub> nanocomposites	813 mAh g <sup>-1</sup> after 100 cycles at 100 mA g <sup>-1</sup>	514 mAh g <sup>-1</sup> at 1 A g <sup>-1</sup>	8
Co <sub>3</sub> O <sub>4</sub> hollow dodecahedrons	1265 mAh g <sup>-1</sup> after 140 cycles at 100 mA g <sup>-1</sup>	650 mAh g <sup>-1</sup> at 2 A g <sup>-1</sup>	9
Co <sub>3</sub> O <sub>4</sub> hollow tetrahedra	1052 mAh g <sup>-1</sup> after 60 cycles at 200 mA g <sup>-1</sup>	606 mAh g <sup>-1</sup> at 0.8 A g <sup>-1</sup>	10
Hollow Co <sub>3</sub> O <sub>4</sub> parallelepipeds	1115 mAh g <sup>-1</sup> after 50 cycles at 100 mA g <sup>-1</sup>	738 mAh g <sup>-1</sup> at 1 A g <sup>-1</sup>	11
Co <sub>3</sub> O <sub>4</sub> nanoplates	852 mAh g <sup>-1</sup> after 100 cycles at 500 mA g <sup>-1</sup>	435 mAh g <sup>-1</sup> at 2 A g <sup>-1</sup>	12
Co <sub>3</sub> O <sub>4</sub> hollow dodecahedra	780 mAh g <sup>-1</sup> after 100 cycles at 100 mA g <sup>-1</sup>	~600 mAh g <sup>-1</sup> at 9 A g <sup>-1</sup>	13

**Table S2.** Comparison of OER performance of Co<sub>3</sub>O<sub>4</sub>-based electrocatalysts

Catalyst & Experimental condition	Overpotential at a current density of 10 mA cm <sup>-2</sup> (mV)	Tafel slope (mV dec <sup>-1</sup> )	References
<b>Co<sub>3</sub>O<sub>4</sub> microframes, 1 M KOH</b>	<b>370</b>	<b>53</b>	<b>This work</b>
Commercial Ir/C	380	Unavailable	14
Mesoporous Co <sub>3</sub> O <sub>4</sub> nanowires, 1 M KOH	~405	72	15
Mesoporous Co <sub>3</sub> O <sub>4</sub> nanoflakes, 1 M KOH	380	48	16
Porous honeycomb-like Co <sub>3</sub> O <sub>4</sub> , 0.1 M KOH	450	89	17
Porous Co <sub>3</sub> O <sub>4</sub> nanoplates, 1 M KOH	~450	71	18
Multiwalled carbon nanotubes/Au/Co <sub>3</sub> O <sub>4</sub> , 1 M KOH	350	68	19
Co <sub>3</sub> O <sub>4</sub> /N-doped porous carbon, 0.1 M KOH	390	72	20
Co <sub>3</sub> O <sub>4</sub> -carbon porous nanowire, 0.1 M KOH	290	70	21
Fe-incorporated mesoporous Co <sub>3</sub> O <sub>4</sub> , 1 M KOH	380	60	22
Co <sub>3</sub> O <sub>4</sub> /multiwalled carbon nanotubes, 0.1 M KOH	390	65	23
Hollow fluffy Co <sub>3</sub> O <sub>4</sub> cages, 1 M KOH	400	70	24
Hollow Co <sub>3</sub> O <sub>4</sub> microspheres, 0.1 M KOH	400	Unavailable	25
nanocast Co <sub>3</sub> O <sub>4</sub> , 0.1 M KOH	496	Unavailable	26
Co <sub>3</sub> O <sub>4</sub> /Co <sub>2</sub> MnO <sub>4</sub> nanocomposites, 0.1 M KOH	540	Unavailable	27
Co <sub>3</sub> O <sub>4</sub> /NiCo <sub>2</sub> O <sub>4</sub> double-shelled nanocages, 1 M KOH	340	88	28
Nanostructured NiCo <sub>2</sub> O <sub>4</sub> , 0.1 M KOH	390	87	29

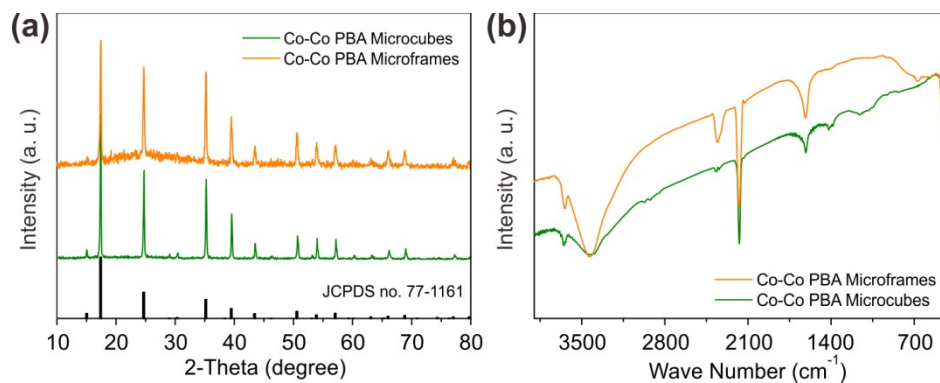


**Fig. S1** XRD patterns (a) and FT-IR spectra (b) of Co-Co PBA microcubes and microframes.

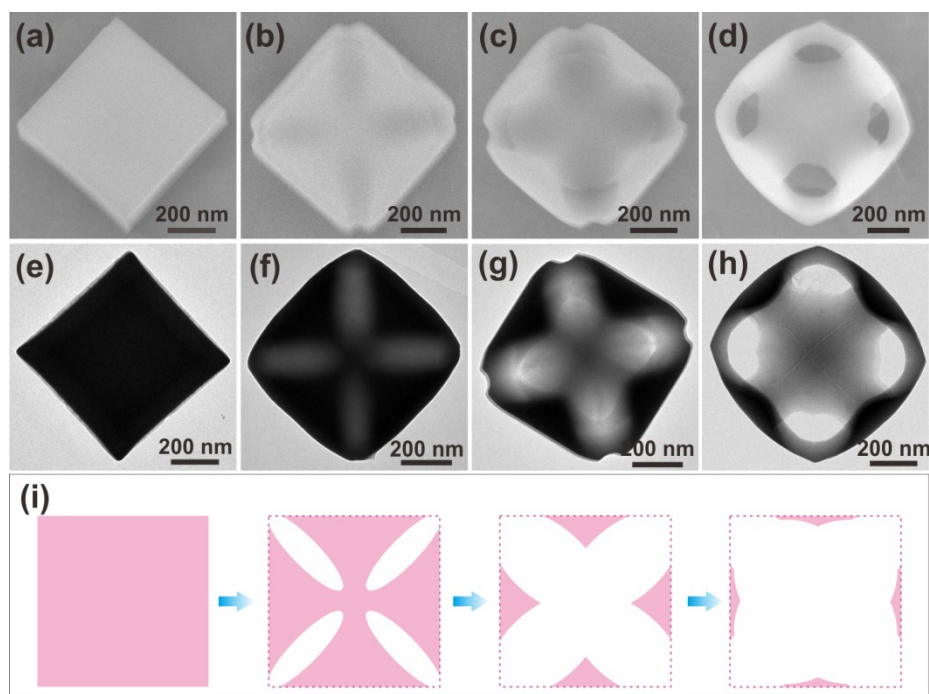


**Fig. S2** SEM images (a-d) and TEM images (e-h) of the as-obtained products after etching with ammonia solution at different time intervals: 0 min (a, e), 3 min (b, f), 5 min (c, g), and 10 min (d, h), respectively. Schematic illustration for the formation process of Co-Co PBA microframes (i-l).

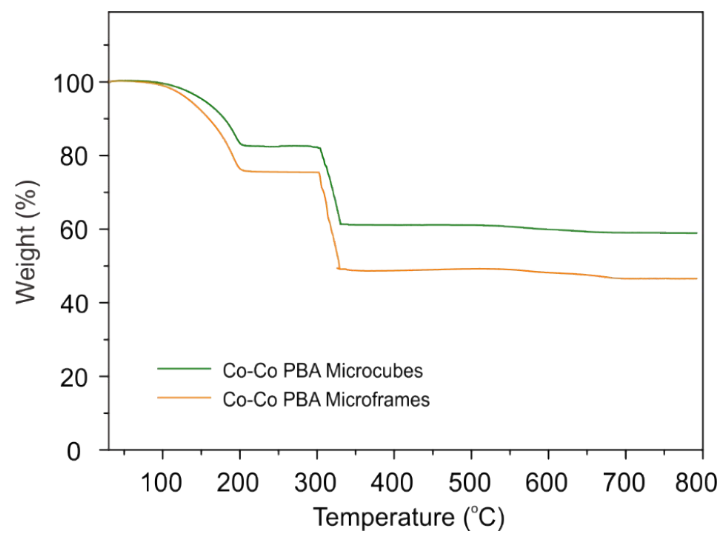


**Fig. S3** TGA curves of Co-Co PBA microframes and microcubes in air in the temperature range from 30 to 800 °C with a heating rate of 10 °C min<sup>-1</sup>.

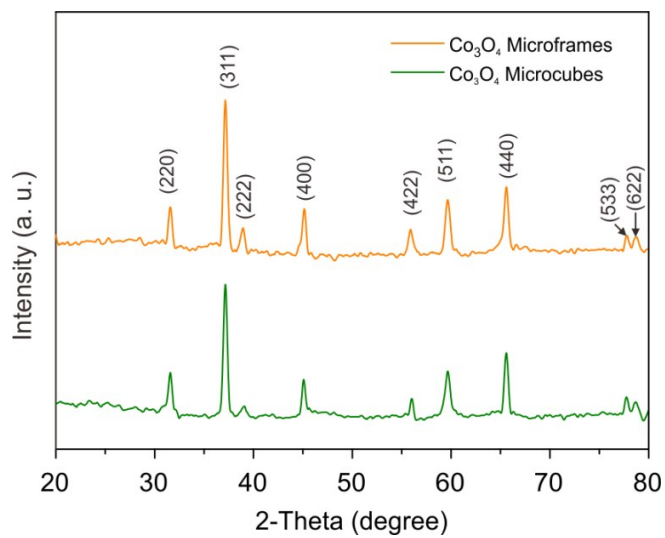


**Fig. S4** XRD patterns of Co<sub>3</sub>O<sub>4</sub> microframes and microcubes.

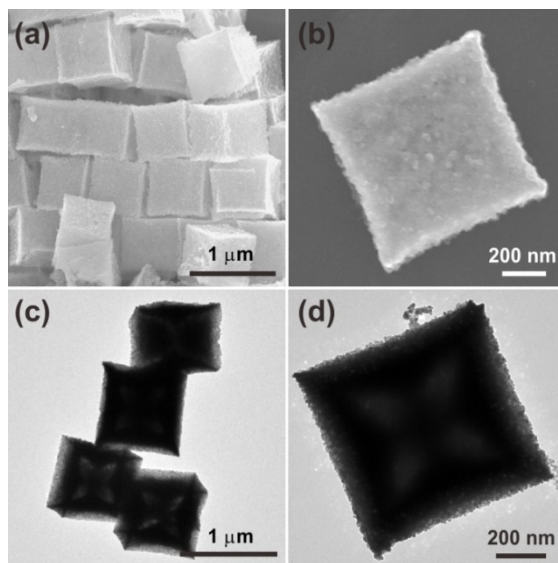


**Fig. S5** SEM images (a-b) and TEM images (c-d) of  $\text{Co}_3\text{O}_4$  microcubes synthesized using Co-Co PBA microcubes as precursor.

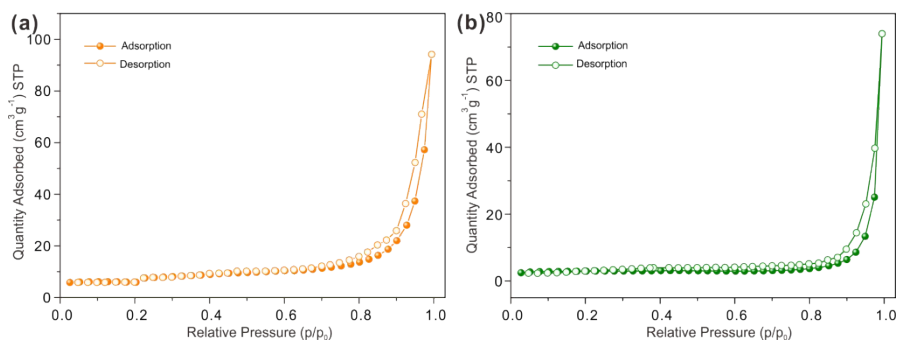


**Fig. S6**  $\text{N}_2$  adsorption and desorption isotherms of  $\text{Co}_3\text{O}_4$  microframes (a) and microcubes (b).

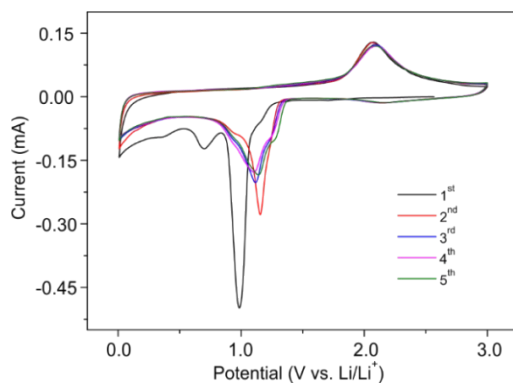


**Fig. S7** CV curves of  $\text{Co}_3\text{O}_4$  microframes for the first 5 cycles at a scan rate of  $0.2 \text{ mV s}^{-1}$ .

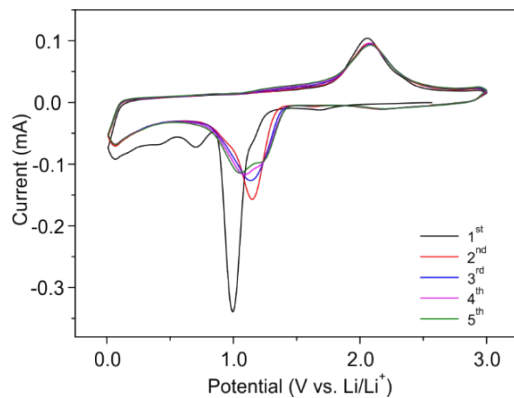


**Fig. S8** CV curves of  $\text{Co}_3\text{O}_4$  microcubes for the first 5 cycles at a scan rate of  $0.2 \text{ mV s}^{-1}$ .

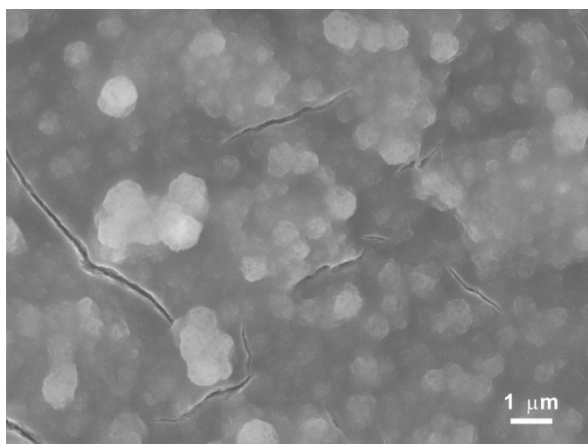


**Fig. S9** SEM image of electrode after cycling test at  $0.5 \text{ A g}^{-1}$  for 200 cycles.

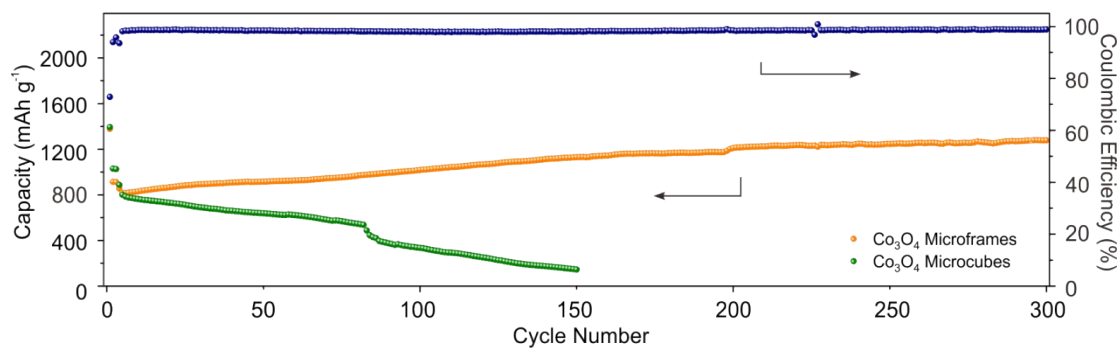


**Fig. S10** Cycling performance of  $\text{Co}_3\text{O}_4$  microframes and microcubes and the corresponding Coulombic efficiency of  $\text{Co}_3\text{O}_4$  microframes at a current density of  $1 \text{ A g}^{-1}$

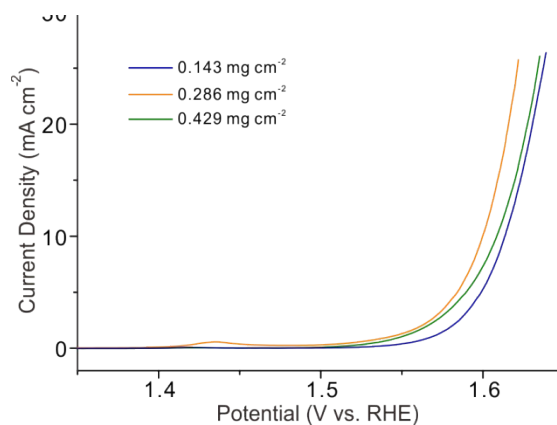


**Fig. S11** Optimization of  $\text{Co}_3\text{O}_4$  microframes electrocatalyst loading on glassy carbon electrode.

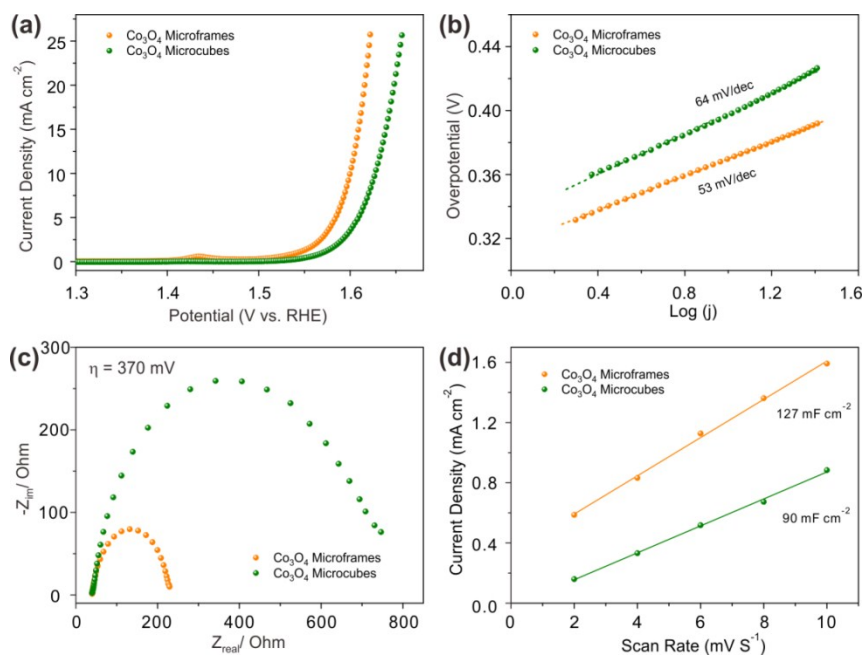


**Fig. S12** LSV curves (a) and Tafel plots (b) of  $\text{Co}_3\text{O}_4$  microframes and microcubes. (c) EIS Nyquist plots of  $\text{Co}_3\text{O}_4$  microframes and microcubes in 1 M KOH at an overpotential of 370 mV; (d) Plots showing the extraction of the  $C_{dl}$  for  $\text{Co}_3\text{O}_4$  microframes and microcubes.

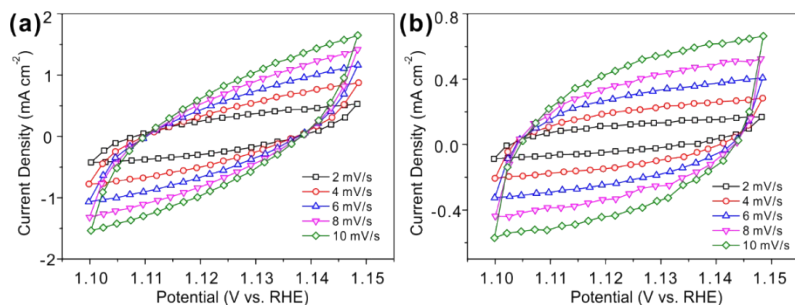


**Fig. S13** CVs in the region of 1.10-1.15 V vs. RHE for Co<sub>3</sub>O<sub>4</sub> microframes (a) and microcubes (b).

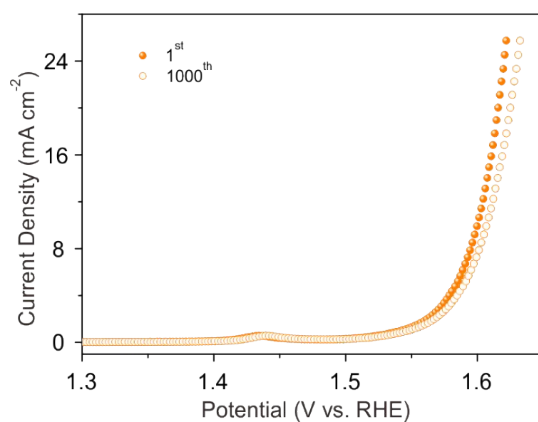


**Fig. S14** Cycling stability of Co<sub>3</sub>O<sub>4</sub> microframes for OER at a scan rate of 50 mV s<sup>-1</sup>.

### Proposed Etching Reaction Mechanism

Chemical etching has been recently used to obtain diverse nanostructures. For example, xylenol orange sodium salt has been utilized as etchant to obtain frame-like and box-like ZIF-8/ZIF-67 nanostructures (*Angew. Chem. Int. Ed.*, 2015, 54, 14417-14421). Huang et al. used ammonia solution as etchant to obtain Cu<sub>2</sub>O with different shapes (*J. Phys. Chem. C*, 2011, 115, 20618-20627). The complexation between Cu<sup>+</sup> and NH<sub>3</sub> to form [Cu(NH<sub>3</sub>)<sub>4</sub>]<sup>+</sup> is believed to be the main etching mechanism. Inspired by this, here we also choose ammonia solution as etchant. The possible reaction mechanism is  $\text{Co}_3[\text{Co}(\text{CN})_6]_2(\text{s}) + \text{NH}_3(\text{aq}) \rightarrow [\text{Co}(\text{NH}_3)_6]^{2+}(\text{aq}) + [\text{Co}(\text{CN})_6]^{3-}(\text{aq})$ . When Co-Co PBA are etched with ammonia solution for longer time, it will be fully etched

away to form brown solution as shown in Fig. S15b. When excess ammonia solution is added to  $\text{Co}^{2+}$  solution (control), complex ion solution with similar brown color is also observed (Fig. S15c), confirming the proposed reaction mechanism.

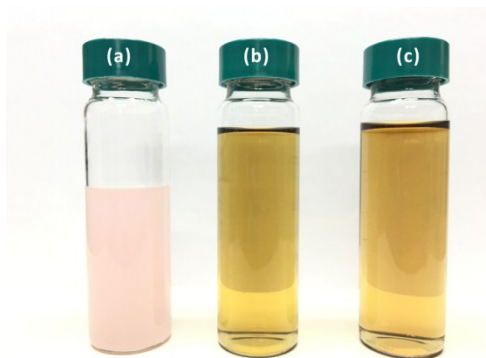


**Fig. S15** (a) Solution of Co-Co PBA; (b) Solution of fully etched out Co-Co PBA using ammonia solution; (c) Complex ion solution of  $\text{Co}^{2+}$  and ammonia.

## References

1. N. Yan, L. Hu, Y. Li, Y. Wang, H. Zhong, X. Y. Hu, X. K. Kong and Q. W. Chen, *J. Phys. Chem. C*, 2012, **116**, 7227-7235.
2. Z. Q. Li, B. Li, L. W. Yin and Y. X. Qi, *ACS Appl. Mater. Interfaces*, 2014, **6**, 8098-8107.
3. B. Liu, X. B. Zhang, H. Shioyama, T. Mukai, T. Sakai and Q. Xu, *J. Power Sources*, 2010, **195**, 857-861.
4. P. P. Su, S. C. Liao, F. Rong, F. Q. Wang, J. Chen, C. Li and Q. H. Yang, *J. Mater. Chem. A*, 2014, **2**, 17408-17414.
5. Y. Wang, B. F. Wang, F. Xiao, Z. G. Huang, Y. J. Wang, C. Richardson, Z. X. Chen, L. F. Jiao and H. T. Yuan, *J. Power Sources*, 2015, **298**, 203-208.
6. Q. T. Qu, T. Gao, H. Y. Zheng, X. X. Li, H. M. Liu, M. Shen, J. Shao and H. H. Zheng, *Carbon*, 2015, **92**, 119-125.
7. C. Li, T. Q. Chen, W. J. Xu, X. B. Lou, L. K. Pan, Q. Chen and B. W. Hu, *J. Mater. Chem. A*, 2015, **3**, 5585-5591.
8. G. Huang, F. F. Zhang, X. C. Du, Y. L. Qin, D. M. Yin and L. M. Wang, *ACS Nano*, 2015, **9**, 1592-1599.
9. J. Shao, Z. M. Wan, H. M. Liu, H. Y. Zheng, T. Gao, M. Shen, Q. T. Qu and H. H. Zheng, *J. Mater. Chem. A*, 2014, **2**, 12194-12200.
10. D. Tian, X. L. Zhou, Y. H. Zhang, Z. Zhou and X. H. Bu, *Inorg. Chem.*, 2015, **54**, 8159-8161.
11. Y. Han, M. L. Zhao, L. Dong, J. M. Feng, Y. J. Wang, D. J. Li and X. F. Li, *J. Mater. Chem. A*, 2015, **3**, 22542-22546.

12. J. X. Guo, B. Jiang, X. Zhang, L. Tang and Y. H. Wen, *J. Mater. Chem. A*, 2015, **3**, 2251-2257.
13. R. B. Wu, X. K. Qian, X. H. Rui, H. Liu, B. L. Yadian, K. Zhou, J. Wei, Q. Y. Yan, X. Q. Feng, Y. Long, L. Y. Wang and Y. Z. Huang, *Small*, 2014, **10**, 1932-1938.
14. Y. Gorlin and T. F. Jaramillo, *J. Am. Chem. Soc.*, 2010, **132**, 13612-13614.
15. Y. C. Wang, T. Zhou, K. Jiang, P. M. Da, Z. Peng, J. Tang, B. A. Kong, W. B. Cai, Z. Q. Yang and G. F. Zheng, *Adv. Energy Mater.*, 2014, **4**.
16. S. Q. Chen, Y. F. Zhao, B. Sun, Z. M. Ao, X. Q. Xie, Y. Y. Wei and G. X. Wang, *ACS Appl. Mater. Interfaces*, 2015, **7**, 3306-3313.
17. L. L. Li, T. Tian, J. Jiang and L. H. Ai, *J. Power Sources*, 2015, **294**, 103-111.
18. X. M. Zhou, Z. M. Xia, Z. M. Tian, Y. Y. Ma and Y. Q. Qu, *J. Mater. Chem. A*, 2015, **3**, 8107-8114.
19. Y. Y. Fang, X. Z. Li, Y. P. Hu, F. Li, X. Q. Lin, M. Tian, X. C. An, Y. Fu, J. Jin and J. T. Ma, *J. Power Sources*, 2015, **300**, 285-293.
20. Y. Hou, J. Y. Li, Z. H. Wen, S. M. Cui, C. Yuan and J. H. Chen, *Nano Energy*, 2015, **12**, 1-8.
21. T. Y. Ma, S. Dai, M. Jaroniec and S. Z. Qiao, *J. Am. Chem. Soc.*, 2014, **136**, 13925-13931.
22. C. L. Xiao, X. Y. Lu and C. Zhao, *Chem. Commun.*, 2014, **50**, 10122-10125.
23. X. Y. Lu and C. Zhao, *J. Mater. Chem. A*, 2013, **1**, 12053-12059.
24. X. M. Zhou, X. T. Shen, Z. M. Xia, Z. Y. Zhang, J. Li, Y. Y. Ma and Y. Q. Qu, *ACS Appl. Mater. Interfaces*, 2015, **7**, 20322-20331.
25. J. Zhao, Y. C. Zou, X. X. Zou, T. Y. Bai, Y. P. Liu, R. Q. Gao, D. J. Wang and G. D. Li, *Nanoscale*, 2014, **6**, 7255-7262.
26. X. H. Deng, W. N. Schmidt and H. Tuysuz, *Chem. Mater.*, 2014, **26**, 6127-6134.
27. D. D. Wang, X. Chen, D. G. Evans and W. S. Yang, *Nanoscale*, 2013, **5**, 5312-5315.
28. H. Hu, B. Y. Guan, B. Y. Xia and X. W. Lou, *J. Am. Chem. Soc.*, 2015, **137**, 5590-5595.
29. M. Prabu, K. Ketpang and S. Shanmugam, *Nanoscale*, 2014, **6**, 3173-3181.